Active Damping of Torsional Interharmonic in Large Variable Speed Drives

Catalin Arghir[1], Amin Rezaeizadeh[1], Pieder Jörg[2] and Silvia Mastellone[1]

***Abstract*— One of the major challenges in the reliable operation of power converters are the harmonics propagated along the electromechanical system. Limited knowledge of the load, whose mechanical characteristics possibly change over time, demand a robust approach to optimally operate the converter. In this work, we present a frequency domain control solution to address oscillation propagation along the drive, improve its performance, reduce the chance of triggered faults and shaft damage.**

I. INTRODUCTION

One of the major challenges in the reliable operation of drives loads are the harmonics and interharmonics generated by Variable Speed Drives (VSDs), that can induce pulsating torque resonating with the natural torsional frequencies of the mechanical system. In systems with low modal damping, those pulsations lead at best to underperformance, and can trigger the tripping mechanism in place to guarantee safe operation, resulting in the shutdown of the entire process. Over time, in some critical cases the persistent torsional oscillation, causes shaft rapture.

In the deployment phase, when a drive is commissioned, the control loops are calibrated empirically with limited knowledge of the process. In particular, the resulting frequency response, and hence the resonant frequency of the interconnected electro-mechanical system is unknown. Additionally, the resonant frequency can shift over time due to the degradation of some mechanical components or changes in the process load [1]. Therefore, careful interoperability considerations have to be taken into account when designing controllers for the electrical drive system and the mechanical drivetrain. Strategies include the design of active damping controllers or the adjustment of operational frequencies to avoid activating the system resonance [2]. In recent years, a number of active damping control algorithms for variable speed drives have been the subject of investigation. These methods use the speed or shaft torque feedback to protect the mechanical components against vibrations [3]–[8]. Some methods are based on adaptive notch filters to cancel the resonance [4, 9]. Others proposed active disturbance rejection based on proportional–resonant (PR) control [10]. In [11], an alternative pulse mode is proposed, in order to keep the excitation of the natural frequencies of the drive shaft at a minimum. Or in [5], an externally applied integrated torsional mode damping (ITMD) control is investigated which is based on torque sensor measurement. A number of control techniques have been used for active damping of underactuated systems, including but not limited to H_∞, model predictive control (MPC) and sliding-modes. However, the uncertainty in modeling actual resonance modes, to properly operate the mechanical load requires a robust approach in the converter control design [12, 13].

In this work, we consider a robust control technique based on *the eigenvalue perturbation* method [14] to control the shaft speed while damping the resonant peaks. The designed controller is then investigated in terms of robust stability using the μ-function.

Additionally, to demonstrate the effect of torsional oscillations stress on the shaft damage, and the effectiveness of the proposed method in reducing the damage effect, we present a fatigue analysis in frequency-domain.

The paper is structured as follows: Section II describes the torsional drive model that will be considered in the paper. Section III presents the proposed H_∞ control strategy and Section IV demonstrates the controller performance on a simulation setup. Section V present a fatigue analysis where the effect of torsional oscillations on shaft damage are studied. Finally the conclusive remarks are presented in Section VI.

II. SYSTEM DESCRIPTION

A. Variable speed drive

We consider a Load Commutated Inverter (LCI) system driving large industrial loads or gas and oil pumps. The system consists of two six-pulse thyristor bridges on both the grid side (rectifier) and the machine side (inverter), resulting in a 12-pulse configuration through phase-shifted windings to reduce voltage ripple (see Fig. **??**). The primary frequencies of the voltage ripple created by the rectifier and inverter bridges correspond to the integer pulsating torque frequencies:

$$f_{\text{pulsating}} = |12 n_g f_g \pm 12 n_m f_m|, \tag{1}$$

where n_g, n_m are integers, f_g is the grid frequency and f_m is the motor electrical frequency, as illustrated in Fig. 2.

B. Torsional drivetrain model

To model the drive, we assume that the current through the DC reactance L_{dc} is controlled by an inner current loop

This work was supported by the Swiss National Science Foundation under NCCR Automation, grant agreement 51NF40_180545

[1]Catalin Arghir, Amin Rezaeizadeh and Silvia Mastellone are with the Institute of Electric Power Systems, University of Applied Science Northwest Switzerland, Windisch, Switzerland. catalin.arghir@fhnw.ch, amin.rezaeizadeh@fhnw.ch, silvia.mastellone@fhnw.ch

[2]Pieder Jörg is with ABB Motion, ABB Switzerland Ltd., Turgi, Switzerland. pieder.joerg@ch.abb.com

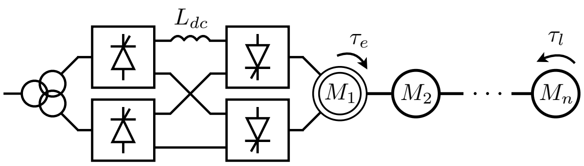

Fig. 1: Schematic of the driveline system, comprising the LCI system, motor and driveline shaft.

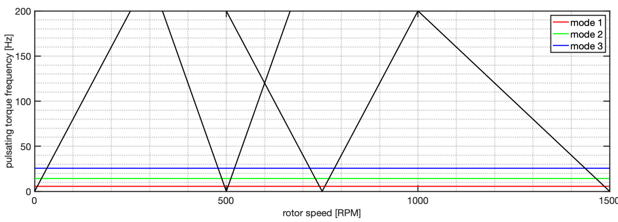

Fig. 2: Campbell diagram of the 12/12-pulse LCI system and the corresponding modal frequencies of the driveline shaft, with resonance occurring at the intersection of modal and pulsating frequencies.

commanding the thyristor firing angles at a sufficiently high rate. The reference for this inductor current is assumed to be directly proportional to the electrical torque produced by the motor. For the remaining of this paper we focus only on the speed control loop that is generating the current reference.

We further model our driveline shaft as a system of n point-masses interconnected by $n-1$ springs according to an incidence matrix E. We restrict ourselves to a line graph with one edge between each consecutive node. Suppose that the angular position of each mass is $\theta_i \in \mathbb{R}$ with the angular velocity $\omega_i = \dot{\theta}_i \in \mathbb{R}$. Let $M = \mathrm{diag}(M_1, \dots M_n)$ be the positive definite mass matrix and $K = \mathrm{diag}(K_1, \dots K_{n-1})$ be the positive definite spring coefficient matrix. In addition, we define the positive definite edge damping matrix as $C = \mathrm{diag}(C_1, \dots C_{n-1})$. Let $\tau_e \in \mathbb{R}$ be the input (drive torque), and let $\tau_l \in \mathbb{R}$ be the disturbance (load torque). We take $\theta = \mathsf{col}(\theta_1, \dots \theta_n)$ and write the Hamiltonian as

$$\mathscr{H}(\theta, \dot{\theta}) = \tfrac{1}{2}\theta^\top \mathscr{L}_K \theta + \tfrac{1}{2}\dot{\theta}^\top M \dot{\theta}\,, \tag{2}$$

where $\mathscr{L}_K = EKE^\top$ is a Laplacian matrix, we see that the stationary locus of the potential energy corresponds to angle consensus. The dynamics take the form of a second order Laplacian flow

$$M\ddot{\theta} + \mathscr{L}_C \dot{\theta} + \mathscr{L}_K \theta = n_1 \tau_e - n_n \tau_l\,, \tag{3}$$

where n_1 and n_n are the first and the last natural basis elements of $\mathbb{R}^n$, and $\mathscr{L}_C = D + ECE^\top$ denotes a loopy Laplacian with a small but nonzero eigenvalue associated with friction $D = \mathrm{diag}(D_1, \dots D_n)$, positive semi-definite. The mechanical system described in (3) may result from a finite-element spatial-discretisation of a solid body (in our case, a driveline shaft), where only one degree-of-freedom is considered: the rotation about an axis, all others being restricted via bearings.

The control setup

The control problem can be posed as follows: command the torque acting on one side the shaft such that all mass elements track the same (reference) velocity r, subject to a disturbance torque acting on the other side of the shaft.

Notice that, in loading conditions, the steady state becomes

$$KE^\top \theta^{\mathsf{ss}} = \mathbb{1}_{n-1}\tau_l\ ,\ \tau_e^{\mathsf{ss}} = \tau_l\,, \tag{4}$$

in other words, the load torque fully propagates throughout the shaft. The dynamic behaviour can be quantified by the so-called Torsional Natural Frequencies (TNFs) and their associated damping factors. The underdamped nature of the system gives rise to high *cycle fatigue* in the shaft, and over time leads to shaft damage. Our proposal is to define the following output as multivariable stressor signal

$$\tau = KE^\top \theta + CE^\top \dot{\theta}\,, \tag{5}$$

and use it for our fatigue spectral estimation approach.

III. Active control of the torsional stress

In order to minimize the shear stress along the shaft, we model the shear stress in each shaft segment [15] as $s_i = \frac{R_i}{J_i}\tau_i$ Where R_i is the radius of the shaft segment, J_i is its polar area moment of inertia, and τ_i is the internal torque, i.e. the torque acting between each segment:

$$\tau_i = K_i\left(\theta_{i+1} - \theta_i\right) + C_i\left(\dot{\theta}_{i+1} - \dot{\theta}_i\right). \tag{6}$$

The internal torque, τ_i, is in fact a response of two external torques acting on the two sides of the shaft, i.e. the motor torque and the load torque. Mathematically, the internal torque can be expressed in terms of τ_e and τ_l as follows:

$$\tau_i = G_{e,i}\tau_e + G_{l,i}\tau_l =: G\begin{pmatrix}\tau_e \\ \tau_l\end{pmatrix}, \tag{7}$$

where $G_{e,i}$ and $G_{l,i}$ are two linear transfer functions that depend on the shaft model parameters, as well as the location of the i^{th} segment.

Figure 3 illustrates the schematic of the closed-loop system design for a shaft with $n = 5$ point-masses. The controller is a multiple-input single-output (MISO) system that provides the air gap torque, τ_e, based on the inputs from the reference and the measured shaft speed. The interharmonics are modeled as additive signal to the controller output and are speed-dependent, as per (1). The control objective is to generate an appropriate air gap torque such that the shaft speed follows the desired speed profile, while the internal torque oscillation is minimized at every segment. Without loss of generality, we consider only the internal torque between mass 1 and 2 as the signal to be minimized in norm, in addition to the speed tracking error. W_e and W_u are two SISO transfer functions that regulate, respectively, the tracking error and the internal torque signal (between mass 1 and 2). By tuning these two weight factors, one can trade off be-tween the speed tracking performance and internal torque damping.

Since there is always discrepancy between the model and the actual system, the closed-loop system can become

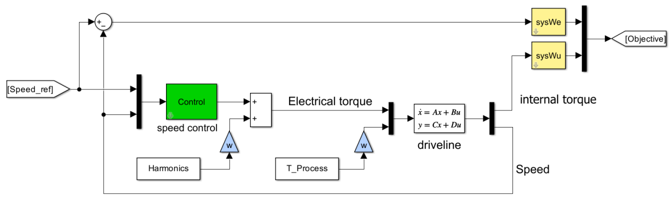

Fig. 3: Closed-loop schematic of the driveline system, comprising the weights for shaping the controller design.

unstable or, in the best case, might not perform as expected, especially around the resonant frequencies. The uncertainty in the driveline's modes can be modeled by perturbation in eigenvalues of the system [14, 16, 17]. In this case, the state matrix A is replaced by

$$A \to A + L\Delta R, \tag{8}$$

where Δ is a full-block complex matrix with a bounded norm, i.e. $\Delta \in \mathbb{C}^{2m\times 2m}$, $\bar{\sigma}(\Delta) \leq 1$, with m being the number of uncertain modes, L and R are the left and right scaling matrices. The matrix A is assumed to have the modal structure with n complex conjugate eigenvalue pairs, $\lambda_{i\pm} = \sigma_i \pm j\beta_i$, as follows:

$$A = \mathrm{blkdiag}(A_{11}, \ldots A_{nn}), \text{ where } A_{ii} = \begin{bmatrix} \sigma_i & \beta_i \\ -\beta_i & \sigma \end{bmatrix}. \tag{9}$$

The L and R scaling matrices have the following block diagonal structures to affect only the eigenvalues that have uncertainty:

$$L = \mathrm{blkdiag}(O_*, W, O_*),\ R = \mathrm{blkdiag}(O_*, I_{2m}, O_*), \tag{10}$$

where W is a weighting matrix that specifies the uncertainty weight (note that norm of Δ is assumed to be less than 1), and has the following diagonal structure:

$$W = \mathrm{blkdiag}(w_1 I_2, \ldots w_m I_2), \quad w_i > 0. \tag{11}$$

From Geršgorin theorem it can be shown that the eigenvalues of $A + L\Delta R$, for all $\bar{\sigma}(\Delta) \leq 1$, are located at the union set of the eigenvalues of A and a set containing m pairs of disks, of radius w_i, centered at the uncertain eigenvalues of A. For more details, the reader is referred to [17, 18].

Figure 4 illustrates the nominal eigenvalues of A (denoted by $*$) and the perturbation disks around each. Note that for some eigenvalues that are very close to the imaginary axis, the associated disk is shifted to the left to avoid capturing unstable modes in the model [14]. The uncertainty in the modes is considered only for the three lowest modes. The driveline dynamics are replaced by the following perturbed state-space model:

$$\begin{aligned} \dot{x}(t) &= \left(\tilde{A} + L\Delta R\right) x(t) + B\tau_e(t) && (12) \\ \begin{bmatrix} \tau_1(t) \\ \omega_1(t) \end{bmatrix} &= Cx(t) + D\tau_e(t), && (13) \end{aligned}$$

where $\tilde{A}$ is similar to matrix A except for some eigenvalues shifted to the left.

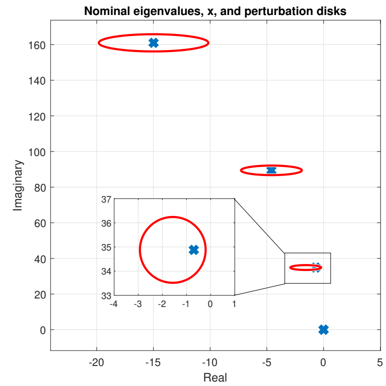

Fig. 4: The first four nominal eigenvalues, denoted by $*$, and the perturbation disks around the first three resonance modes, i.e. $m = 3$. The inset plot shows only the first TNF with the 1:1 aspect ratio.

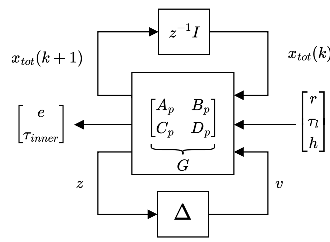

Fig. 5: The LFT representation of the closed-loop system containing the perturbation block, Δ.

We convert the control system diagram (depicted in Fig. 3) into a linear fractional transformation (LFT) form as illustrated in Fig. 5. The static parameters of the driveline, the controller and the weighting functions are all embedded in a constant G matrix, while their state variables are all captured by x_{tot}. To construct the optimal controller, we look for a discrete-time control transfer function $K(z)$ that minimizes the H_∞ norm of the closed-loop transfer function from the external inputs to the penalized outputs for all perturbations up to size one, i.e. $\|\Delta\| \leq 1$. The external inputs are the reference, r, the load torque, τ_l, and the harmonics generated by the power converter which are modeled here as an additive disturbance, denoted by h. The penalized outputs are the speed tracking error, e, and the internal torque between mass 1 and 2, i.e. τ_1.

The design procedure is as follows (known as the D-K iteration [19, 20]):

1) An H_∞ controller is designed for the nominal case (i.e. $\Delta = 0$)
2) Calculate the μ upper bound and its corresponding D-scaling [21, 22]:

$$\mu_{\Delta_s}(G) \leq \bar{\sigma}(D_s G D_s^{-1}), \tag{14}$$

where μ is the structured singular value operator, D_s is the constant D-scaling matrix that commutes with the block structure Δ_s that is defined as follows:

$$\Delta_s := \left\{ \text{diag}\left(\delta_1 I_*,\ \Delta_p,\ \Delta\right) \middle| \delta_1 \in \mathbb{C},\ \Delta_p \in \mathbb{C}^{3\times 2}, \right.$$
$$\left. \Delta \in \mathbb{C}^{2m\times 2m} \right\} \quad (15)$$

3) The computed D-scaling matrix is applied to the system and a new H_∞ controller is designed. This time, as $\Delta \neq 0$, the signals v and z are included, respectively, in the system input and output for the control design.

The resulting closed-loop system is then analyzed again in step 2 and the iterations take place between steps 2 and 3 until the μ-upper bound is sufficiently reduced below one. The controller designed in step 1, i.e. the nominal case, will be used as the baseline to compare the performance of the μ-synthesis controller.

IV. Simulation Results

A. Frequency-domain analysis

In the previous section, we modeled the uncertainty in the modes as a complex full-block matrix without any imposed structure. However, one could consider a real perturbation model with a specific structure. Since the dynamics of the system are real, any perturbation of an eigenvalue of the nominal state matrix A must have the same effect on its complex conjugate (and vice-versa). This imposes the following structure for real Δ:

$$\Delta_{ii} = \begin{bmatrix} \delta_{i1} & \delta_{i2} \\ -\delta_{i2} & \delta_{i1} \end{bmatrix}, \quad \delta_{i1}, \delta_{i2} \in \mathbb{R} \quad (16)$$

where Δ_{ii} corresponds to the A_{ii} block defined in (9).

As explained in [16], both perturbation models, i.e. taking a full block complex matrix or a real one, give an identical result. Nevertheless, here we use the real perturbation with the imposed structure, as it is realistic, just to illustrate the robust stability of the closed-loop system. For the μ-synthesis design, however, we use the procedure described in the previous section, as it is computationally efficient. Figure 6 illustrates the μ function of the robust stability of the closed-loop system versus frequency for the H_∞ and the μ-synthesis designs. As we can see, the closed-loop system is stable with both designs ($\mu < 1$ at all frequencies), with some spikes at around the resonance frequencies. With the μ-synthesis, however, the peaks are lowered which corresponds to more stability robustness against uncertainty in the modes. Figure 7 plots the magnitude of the transfer function from harmonics to the internal torque for different systems. The sampling time of the discrete-time controller is $50\mu s$. In comparison to the open-loop system, applying the H_∞ control, results in a shift of the first resonance peak to a lower frequency and with high damping factor. For the second resonance peak, we can see a slight degree of dampening. With the μ-synthesis control, however, all three resonance peaks are significantly lowered down. In terms of the closed-loop tracking bandwidth, both controllers perform similarly, as shown in Fig. 8, with the bandwidth of approximately 4rad/s. Regarding the load torque disturbance rejection, while

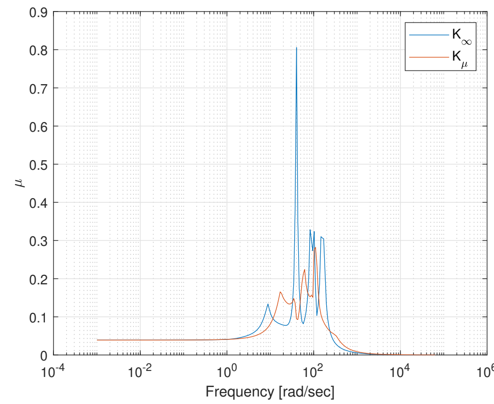

Fig. 6: Robust stability analysis of the two control methods on real structured uncertainty in the resonance modes.

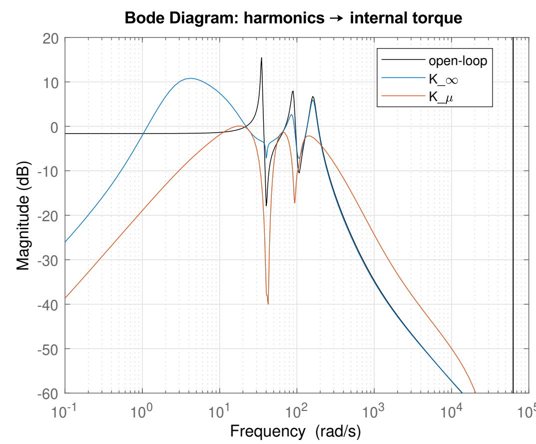

Fig. 7: The magnitude of the open-loop and closed-loop transfer functions from the harmonics to the internal torque between mass 1 and 2.

both controllers show relatively low values, the μ-synthesis method effectively eliminates the resonance peaks.

B. Time-domain response

In this simulation, we test performance of both controllers against speed reference tracking and resonance dampening at the internal torques. The reference profile is a ramp, simulating a startup of a variable-speed drive system. During this process, the driveline can experience torsional vibrations due to interference of the harmonics frequency content and the resonance frequencies of the mechanical system.The harmonics generated in the drive torque vary with the rotor speed and are simulated according to Fig. 2.

Figure 9 illustrates the ramp response of the system for both control methods. The upper plot depicts the speed tracking response. The load torque is assumed to be constant. As we can see, both controllers achieve the same level of performance in tracking the ramp profile, which was previously expected based on the closed-loop bandwidth observed in Fig. 8. The lower plot shows the internal torques during the ramp-up for both controllers. Clearly, the μ-synthesis control

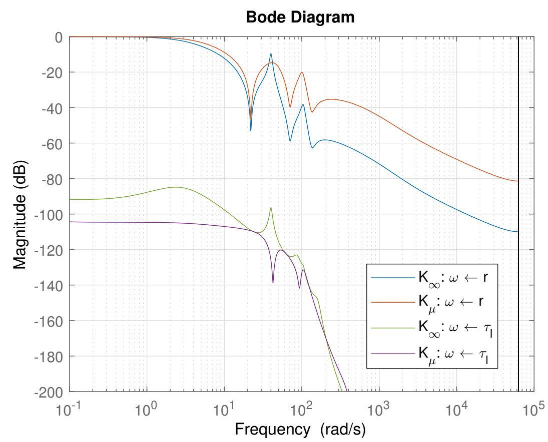

Fig. 8: The magnitude of the closed-loop reference tracking and disturbance rejection transfer functions.

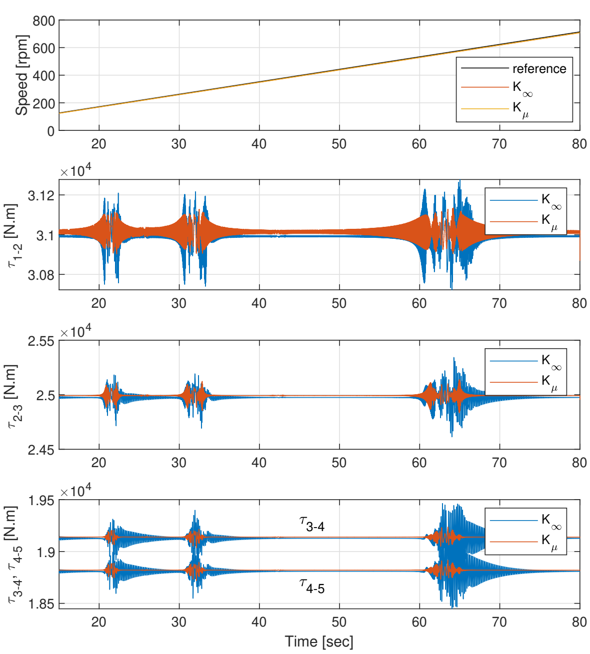

Fig. 9: Time-domain simulation of the closed-loop system to a ramp speed profile.

method significantly reduces the resonances occurring during the ramp-up, as expected from the frequency domain analysis in Fig. (7). The following section will present the results of the fatigue analysis, which will demonstrate how these internal torque oscillations translate to accumulated damage.

V. Fatigue Analysis

Next we analyze the effect of torsional oscillation on the mechanical damage experienced by the shaft, and demonstrate how the proposed controller contribute to significantly reducing damaging effect of the torsional oscillations. We consider a fatigue model expressed as the relationship between the stress amplitude and the number of cycles-to-failure. The accumulated damage D_{tot} experienced by a system for one cycle of operation can be determined as

$$D_{\text{tot}} = \sum_{i=1}^{n} \frac{n(S_i)}{N_f(S_i)}, \tag{17}$$

where $n(S_i)$ denotes the experienced number of cycles of amplitude S_i, and $N_f(S_i)$ denotes the available number of cycles empirically derived as the material S-N curve. This relationship takes the form of a power law, $N_f(S_i) = \alpha S_i^{\kappa}$, where κ and $\log \alpha$ are, respectively, the slope and offset of the S-N curve in logarithmic scale. When D_{tot} reaches one, failure is expected to occur. To estimate the effective number of cycles $n(S_i)$ experienced at a corresponding to stress level S_i, the stress signal is processed using a cycle counting method, most commonly the rainflow counting (RFC) algorithm [23]. The fatigue analysis literature consists of a wealth of RFC approximation methods [24]–[26]. In our mechanical driveline, the stress cycles are assumed to be nearly sinusoidal, making it possible to apply statistical methods to predict the number of cycles and their respective amplitudes.

A. Fatigue Damage Spectrum

We adopt the Single Moment Method [25] applied within the narrow band approximation framework. We evaluate the instantaneous damage by using the i^{th} component of the Power Spectral Density (PSD) of the stressor signal as

$$d_i = \nu_{0,i}(2\lambda_{0,i})^{-\frac{\kappa}{2}} \alpha^{-1} \Gamma(1 - \tfrac{m}{2}) \tag{18}$$

where $\nu_{0,i} = \frac{1}{2\pi}\omega_i$ is the frequency band, $\lambda_{0,i} = P(\omega_i)\mathrm{d}\omega$ is the variance associated to the i^{th} component of the PSD of the signal, denoted by P, and $\mathrm{d}\omega$ is the frequency bin, while Γ is the gamma function, accounting for the narrow band approximation. In this way, the spectrum of the stressor signal can be mapped into a Fatigue Damage Spectrum (FDS) in order to evaluate the most harmful frequency components. As we see from Fig. 10, the damage spectrum as well as the fatigue resulting from the RFC algorithm are both improved by the μ-synthesis approach.

VI. Conclusion

In this work we focused on enabling efficient and reliable operation of power converters driving large loads at the core of industrial processes. Specifically, we addressed one the major challenges in their reliable operation, that is the harmonics propagated along the electromechanical system that contribute to reduced performance, unplanned process shutdown, and damages shafts. We proposed a robust frequency domain approach to detect and actively damp the oscillations without compromising system dynamic response hence, improving the drive performance, while significantly reducing the chance of triggered faults. The results are currently demonstrated in an high fidelity simulation environment and will be subsequently tested in an hardware in the loop demonstrator. Moreover a fatigue analysis show the

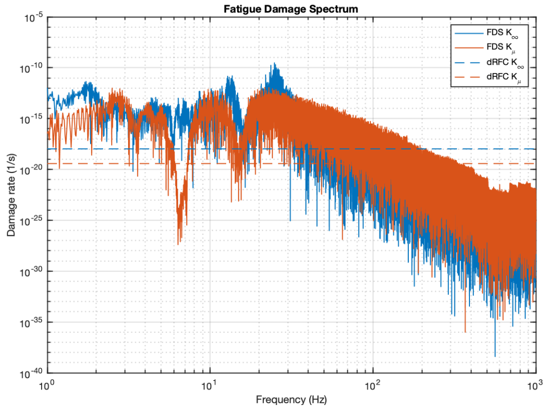

Fig. 10: Fatigue damage spectrum and damage resulting from the RFC in a 70 second interval of ramp-up for the first torque signal in two cases considered.

potential of reducing the shaft damage caused by torsional oscillations.

References

[1] A. Rezaeizadeh and S. Mastellone, "Fast and efficient estimation of resonant modes: A case study of mechanical drivelines," 2024. [Online]. Available: https://arxiv.org/abs/2409.00123

[2] P. Jörg, A. Lenzi, and V. Depau, "Optimization of transient behavior of complex turbocompressor shaft lines," in *2011 IEEE Industry Applications Society Annual Meeting*, 2011, pp. 1–13.

[3] M. Mercangöz, S. Mastellone, S. Almér, T. Besselmann, P. Jörg, J. Niiranen, L. Peretti, and V.-M. Leppänen, "Twist off: Damping torsional oscillations at the intersection of variable-speed drives and elastic mechanical systems," *ABB Review*, vol. 1, pp. 41–47, 2016.

[4] X. Liu, Y. Qi, Y. Tang, Y. Guan, P. Wang, and F. Blaabjerg, "Unified active damping control algorithm of inverter for lcl resonance and mechanical torsional vibration suppression," *IEEE Transactions on Industrial Electronics*, vol. 69, no. 7, pp. 6611–6623, 2022.

[5] S. Schramm, C. Sihler, J. Song-Manguelle, and P. Rotondo, "Damping torsional interharmonic effects of large drives," *IEEE Transactions on Power Electronics*, vol. 25, no. 4, pp. 1090–1098, 2010.

[6] G. Mandic, A. Nasiri, E. Muljadi, and F. Oyague, "Active torque control for gearbox load reduction in a variable-speed wind turbine," *IEEE Transactions on Industry Applications*, vol. 48, no. 6, pp. 2424–2432, 2012.

[7] K. Szabat and T. Orlowska-Kowalska, "Vibration suppression in a two-mass drive system using pi speed controller and additional feedbacks—comparative study," *IEEE Transactions on Industrial Electronics*, vol. 54, no. 2, pp. 1193–1206, 2007.

[8] J. K. Kambrath, C. Yoon, J. Mathew, X. Liu, Y. Wang, C. J. Gajanayake, A. K. Gupta, and Y.-J. Yoon, "Mitigation of resonance vibration effects in marine propulsion," *IEEE Transactions on Industrial Electronics*, vol. 66, no. 8, pp. 6159–6169, 2019.

[9] Y. Chen, M. Yang, J. Long, K. Hu, D. Xu, and F. Blaabjerg, "Analysis of oscillation frequency deviation in elastic coupling digital drive system and robust notch filter strategy," *IEEE Transactions on Industrial Electronics*, vol. 66, no. 1, pp. 90–101, 2019.

[10] G. Shen, X. Zhu, J. Zhang, and D. Xu, "A new feedback method for pr current control of lcl-filter-based grid-connected inverter," *IEEE Transactions on Industrial Electronics*, vol. 57, no. 6, pp. 2033–2041, 2010.

[11] T. J. Besselmann, S. Almér, and P. Jörg, "Torque harmonic minimization for load commutated inverters in pulse mode," *IEEE Transactions on Industrial Electronics*, vol. 65, no. 1, pp. 86–93, 2018.

[12] L. Ovalle, H. Ríos, and H. Ahmed, "Robust control for an active suspension system via continuous sliding-mode controllers," *Engineering Science and Technology, an International Journal*, vol. 28, p. 101026, 2022. [Online]. Available: https://www.sciencedirect.com/science/article/pii/S2215098621001385

[13] T. Yang, N. Sun, and Y. Fang, "Adaptive fuzzy control for a class of mimo underactuated systems with plant uncertainties and actuator deadzones: Design and experiments," *IEEE Transactions on Cybernetics*, vol. 52, no. 8, pp. 8213–8226, 2022.

[14] R. Smith, C.-C. Chu, and J. Fanson, "The design of h/sub /spl infin// controllers for an experimental non-collocated flexible structure problem," *IEEE Transactions on Control Systems Technology*, vol. 2, no. 2, pp. 101–109, 1994.

[15] M. I. Friswell, J. E. T. Penny, S. D. Garvey, and A. W. Lees, *Dynamics of Rotating Machines*, ser. Cambridge Aerospace Series. Cambridge University Press, 2010.

[16] R. Smith, "Eigenvalue perturbation models for robust control," *IEEE Transactions on Automatic Control*, vol. 40, no. 6, pp. 1063–1066, 1995.

[17] ——, "Eigenvalue perturbation models for uncertain structures: A simulation study," Jet Propulsion Laboratory, Tech. Rep. JPL D-9809, May 1992.

[18] ——, "Modeling real parameter variations in flexible structures with complex valued perturbations," in *Proceedings of Conference on Decision and Control*, 1991, p. 1638–1639.

[19] A. Packard and J. Doyle, "The complex structured singular value," *Automatica*, vol. 29, no. 1, pp. 71–109, 1993. [Online]. Available: https://www.sciencedirect.com/science/article/pii/000510989390175S

[20] D. J. G. K. P. A. S. R. Balas, G.J., "μ-analysis and synthesis toolbox," *(No Title)*, 2001.

[21] P. M. Young, M. P. Newlin, and J. C. Doyle, "Practical computation of the mixed μ problem," in *1992 American Control Conference*, 1992, pp. 2190–2194.

[22] A. Packard, M. Fan, and J. Doyle, "A power method for the structured singular value," in *Proceedings of the 27th IEEE Conference on Decision and Control*, 1988, pp. 2132–2137 vol.3.

[23] E. ASTM *et al.*, "Standard practices for cycle counting in fatigue analysis," *Standard Practices for Cycle Counting in Fatigue Analysis*, 2011.

[24] C. E. Larsen and T. Irvine, "A review of spectral methods for variable amplitude fatigue prediction and new results," *Procedia Engineering*, vol. 101, pp. 243–250, 2015.

[25] D. Benasciutti, A. Cristofori, and R. Tovo, "Analogies between spectral methods and multiaxial criteria in fatigue damage evaluation," *Probabilistic Engineering Mechanics*, vol. 31, pp. 39–45, 2013.

[26] M. Muñiz-Calvente, A. Álvarez-Vázquez, F. Pelayo, M. Aenlle, N. García-Fernández, and M. J. Lamela-Rey, "A comparative review of time-and frequency-domain methods for fatigue damage assessment," *International Journal of Fatigue*, vol. 163, p. 107069, 2022.